Research article

Development of a photoacoustic acquisition system and their proof-of-concept for hemoglobin detection

Bruna Pinheiro [a,b], Vânia Pinto [a,b], Hugo Dinis [a,b], Michael Belsley [c], Susana Catarino [a,b], Graça Minas [a,b], Paulo Sousa [a,b],[ID],*

[a] Center for MicroElectromechanical Systems (CMEMS), University of Minho, Guimarães, 4800-058, Portugal
[b] LABBELS — Associate Laboratory in Biotechnology and Bioengineering and Microelectromechanical Systems, University of Minho, Braga, 4710-057, Portugal
[c] Centre of Physics of Minho and Porto Universities (CF-UM-UP), Laboratory for Materials and Emergent Technologies (LAPMET), University of Minho, Braga, 4710-057, Portugal

ARTICLE INFO

ABSTRACT

Recently, Organ-on-a-Chip (OoC) platforms have arisen as an increasingly relevant experimental tool for successfully replicating human physiology and disease. However, there is a lack of a standard technology to monitor the OoC parameters, especially in a non-invasive and label-free way. Photoacoustic (PA) systems can be considered an alternative and accurate assessment method for OoC platforms. PA systems combine an illumination source to excite the sample molecules, with an ultrasound sensor to measure the generated ultrasonic waves, combining the advantages of optics and acoustic methodologies to safely acquire tridimensional signals and images at various depths.

This work is focused on the design, implementation and test of an acquisition electronics circuit, based on the PA principle, for hemoglobin (Hb) detection, aiming towards a future integration within an OoC platform. Based on the measured frequency response of commercial piezoelectric transducers, an electronics design comprising a differential charge amplifier and a band-pass filter was developed. Experimentally it was verified Hb detection for concentrations of Hb between 2.5 and 10 mg/mL in aqueous solutions, roughly 48 times lower than the typical *in vivo* blood concentrations. This creates the possibility of developing this technique to monitor Hb at low concentrations in small volumes, which is highly appropriate for OoC devices.

1. Introduction

An OoC is a system that contains cells, tissues or organ models, natural or artificial, grown inside microfluidic channels. The main purpose of an OoC is the simulation of the physiological environments of human tissues and organs, and one of its greatest potential applications is to assess the safety of drugs before they enter clinical trials, increasing the efficiency of pharmaceutical development.
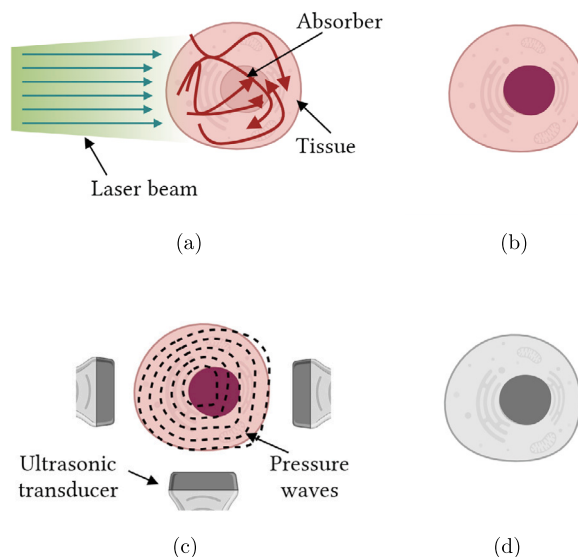

Fig. 1. Schematic representation of the photoacoustic imaging principle. (a) Laser beam excitation (b) Increase of the local temperature (c) Rise and propagation of the pressure wave (d) Image reconstruction from the pressure waves (adapted from [10]).

Therefore, these chips are designed to control the microenvironment of cells while maintaining organ/tissue functioning. By being able to combine advances in tissue engineering with nano and microfabrication, these OoC platforms can be considered the next-level systems for studying both human pathophysiology and therapeutics effects [1,2].

Hemoglobin is one of the molecules essential to monitor on these platforms. Hb is an oxygen-transport metalloprotein in the red blood cells (erythrocytes) of almost all mammals, which plays a significant role in oxygen-carrying processes and is also a typical biomarker for certain diseases [3,4]. This biomolecule, found in the red blood cells of nearly all mammals, is a metalloprotein responsible for carrying oxygen and is a typical biomarker for specific illnesses. Normal levels of hemoglobin in healthy tissues are around 120 to 160 mg/mL in blood cells and below 0.04 mg/mL in human serum [3]. Specific diseases such as heart disease, leukemia, anemia, and others can be closely linked to abnormal levels of hemoglobin in the blood [5]. Currently, several methods such as electrochemical assay, luminescence, chromatography, mass spectrometry and enzyme-linked immunosorbent assay, have been developed for Hb monitoring. However, these methods are expensive and involve multiple preconditioning steps and are not suitable for integration in OoC platforms. In addition, these methods have been limited by the low sensitivity and specificity, requiring bulky and expensive equipment [6,7]. Thus, the development of low cost, non-invasive, highly specific and label-free detection methodologies, able to be integrated into OoC platforms, is crucial.

Nonetheless, a persistent challenge with OoC platforms remains the absence of an integrated and reliable monitoring method, crucial for providing real-time information on Hb distribution.

PA systems can be considered as an alternative and accurate monitoring method in OoC platforms. The measurement of blood's Hb through photoacoustic methods has been clearly validated in the literature [8]. Hb has its dominant optical absorption coefficient at wavelengths below 1000 nm, making it clearly distinguishable from other molecules, such as water and lipids, and allowing it to obtain a photoacoustic contrast for this analyte. The specificity of photoacoustic systems is obtained by the right choice of the excitation wavelength, assuring maximum absorption peaks distinct from other biomolecules. Regarding Hb, the 532 nm excitation wavelength is often considered for imaging Hb with high specificity and a strong photoacoustic effect.

PA systems are hybrid systems that employ an illumination source to excite the sample, producing ultrasonic waves detected by an ultrasound transducer. This non-invasive and label-free biomedical imaging modality leverages the optimal features of both optics and acoustics, enabling the safe acquisition of one-dimensional signals and images across various scales (including organelles, tissues and organs), and with no need for ionizing radiation. Consequently, its primary benefit is the ability to gather information from the sample, as functional and molecular related, without disrupting the regular growth of cells within the OoC.

The PA effect occurs when a tissue surface is exposed to electromagnetic waves, in the intensity-modulated continuous or pulsed form [9]. Following this exposure, the light penetrates the tissue target up to a specific depth, according to its wavelength. The absorption of photons, followed by chromophores' nonradiative relaxation, leads to a swift rise in the temperature, causing the absorbing object to undergo thermoelastic expansion. The abrupt increase in pressure causes the generation and propagation of a sound wave, detectable by traditional ultrasound transducers (Fig. 1). Locating the sources of the pressure waves enables the identification of the specific position of the absorbed light by the sample or tissue, which provides crucial molecular and functional details of the sample.

This work presents the development of a first prototype of the PA detection module (including sensors and instrumentation) and its experimental validation for hemoglobin detection. It is a proof-of-concept, as it aims to be the first step in the development of a novel PA device, suitable to future integration into an OoC.

For that purpose, a theoretical, electrical, and experimental characterization of a commercial lead zirconate titanate (PZT) transducer for the PA detection will be conducted. Piezoelectric transducers are widely used in literature for their well-established fabrication technology and scalable sensitivity [11], making them a simple and cheap option for our proof-of-concept.

2. Theory

To properly excite the sample and efficiently generate broadband PA signals, the duration of the light pulse should be shorter than the times required for thermal and stress relaxation. The thermal relaxation time, which describes the thermal diffusion within a given area, can be approximated by $\tau_{th} = d_c^2/\alpha_{th}$, where α_{th} represents the thermal diffusivity, while d_c denotes the heated area characteristic dimension or the desired spatial resolution. Additionally, the stress relaxation time characterizes how the pressure waves propagate through the domain, being defined by the $\tau_s = d_c/c$, where c represents the speed of sound [9,12]. Generally, pulsed lasers with nanosecond or picosecond peak duration are used as light sources for photoacoustic (PA) imaging to meet the requirements of both thermal and stress confinements [14].

Following excitation, the expansion of fractional volume, which is given by dV/V, can be expressed as

$$\frac{dV}{V} = -\kappa p + \beta T \tag{1}$$

where κ represents the isothermal compressibility of the medium, β represents the thermal coefficient of volume expansion, p represents pressure while T denotes the temperature. Assuming that both thermal and stress induced expansion are confined, it can be assumed that the fractional volume expansion can be neglected, leading to an immediate accumulation of pressure in the heated area. The initial rise of pressure, p_0, is given by Equation (1)

$$p_0 = \frac{\beta T}{\kappa} \tag{2}$$

or described as

$$p_0 = \frac{\beta}{\kappa} \frac{\eta_{th} A_e}{\rho C_v} \tag{3}$$

where A_e denotes the specified optical absorption, η_{th} relates to the optical energy absorbed and converted into heat (in percentage), ρ represents the density of the medium while C_v represents the specific heat capacity at a constant volume. The Gruneisen coefficient, which is a dimensionless thermodynamic constant, defines the efficiency of the heat-pressure conversion, allowing to simplify Equation (3)

$$\Gamma = \frac{\beta}{\kappa \rho C_v} \tag{4}$$

By replacing the Gruneisen coefficient Γ in Equation (3), it becomes

$$p_0 = \Gamma \eta_{th} A_e \tag{5}$$

In the specific conditions of linear optical absorption, i.e., when the local optical fluence F and A_e are proportional, p_0 can be given by:

$$p_0 = \Gamma \eta_{th} \mu_a F \tag{6}$$

where μ_a is the coefficient of optical absorption. Pressure within the heated area immediately rises as a result of the laser's swift energy delivery. This pressure release (as a consequence of thermoelastic expansion), leads to the production of ultrasound waves, when both the thermal linearity and confinement conditions are met.

The following wave equation governs the acoustic pressure of the ultrasonic wave [9,13,15]

$$\left(\nabla^2 - \frac{1}{c^2} \frac{\partial^2}{\partial t^2} \right) p = -\frac{\beta}{C_p} \frac{\partial H}{\partial t} \tag{7}$$

where, C_p represents specific heat capacity, H is the heating function (given by the heat deposited per volume and time units), and is related to A_e through $H = \eta_{th} \frac{\partial A_e}{\partial t}$ [9,15].

Additionally, one of the steps in this work was to characterize different piezoelectric transducers to understand their behavior. Therefore, one of the most important parameters under study is the resonance frequency of the piezoelectric transducer. The resonance frequency (f_r) refers to the natural frequency of vibration or oscillation of an object, where the amplitude or intensity is maximum (and with lower energy losses) [16]. This frequency influences the efficiency of the mechanical wave transmission and is reliant on the transducer's thickness, being given by

$$f_r = n(c/2t_m) \tag{8}$$

where c is the speed of sound in the medium, t_m is its thickness, and n describes an odd integer that represents which odd multiple of a half wavelength is being considered, where $n = 1$ represents the resonance frequency of the material.
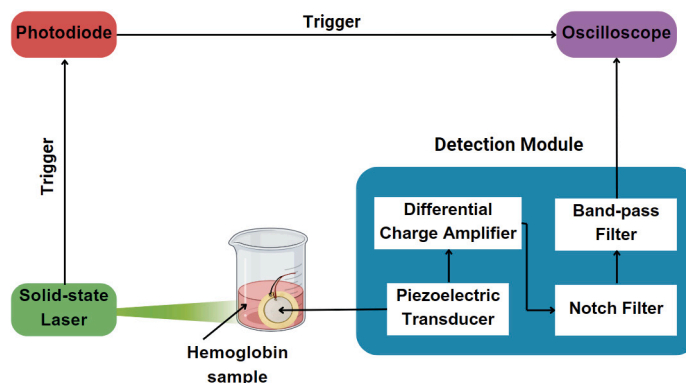
Fig. 2. Illustration of the developed PA system.

3. Methods

3.1. Selection of the piezoelectric transducer

For proceeding for the transducers' characterization, two commercial piezoelectric disks of lead zirconate titanate (PZT) with approximately 27 mm of diameter and 500 μm of thickness were chosen [17].

3.2. Setup for the transducer characterization

In order to perform the electrical characterization of the piezoelectric transducers, a pre-calibrated Vector Network Analyzer (VNA) from Keysight (E5071C) was used. For each frequency in the kHz range, from 10 kHz up to 5 MHz, the transducers' return loss (RL) was evaluated.

Each of the PZT-5H transducers has two metallic contacts which were coated with an acrylic resin (Plastik70 Kontakt Chemie) to block the flow of current through the water medium where the transducers were immersed. Additionally, a pair of wires assures the connection to the testing equipments.

Experimental characterization was carried out to investigate the correlation between the intensity of the emitted and received waves, and to analyze how variations in frequency and the distance between the two transducers affect the received amplitude. Therefore, two piezoelectric disks were placed underwater in a glass container (10 × 8 × 7 cm), enabling a better transmission of the produced mechanical vibrations. Then, a signal generator from Multicomp (MP750065) and a digital oscilloscope (Rigol, DS1102E) were employed to generate the waves and capture the emitted and received waves, respectively. More detail about the setup used for the electrical and experimental characterization of the piezoelectric transducers can be found in [17].

3.3. Experimental setup for the PA system test

To validate the PA system, several concentrations of Hb solutions (in water) were employed. The tests were performed with human Hb obtained from Sigma-Aldrich (H7379, lyophilized powder), since the main target of the application is monitoring human cells in OoC platforms. Using this solution allows us to keep the low cost of the tests and ensure reproducibility.

In order to make PA signal tracking easier, the oscilloscope was synchronized with a signal from a photodiode (trigger), indicating the instant of the laser's light pulse emission. Subsequently, a goblet containing a hemoglobin solution was positioned in the laser's path. The piezoelectric disk, connected to the remaining detection circuit (detailed in section 4.1.2), was placed within the solution with an angle that avoids the laser hitting (approximately 45°). Fig. 2 illustrates the schematic representation of the system setup. The tests were then conducted and the acoustic response was recorded.

4. Photoacoustic system design and implementation

4.1. System design

4.1.1. Illumination source

To excite the sample under study, an illumination source with a wavelength in the 400-600 nm range (hemoglobin has maximum absorption at 414, 541 and 576 nm wavelengths [18]), a narrow pulse width, and an energy level of around mJ was required for our PA system. Consequently, a solid-state laser was selected. The Nd:YAG laser (LPY604T-10, Litron Lasers) (Figs. 3 (a) and (b)) emitted light pulses into the PA system, with a wavelength of 532 nm, 10 Hz PRF, 20 ns pulse width, and 1.2 mJ of energy per pulse, focusing on an area of 60 μm in diameter.
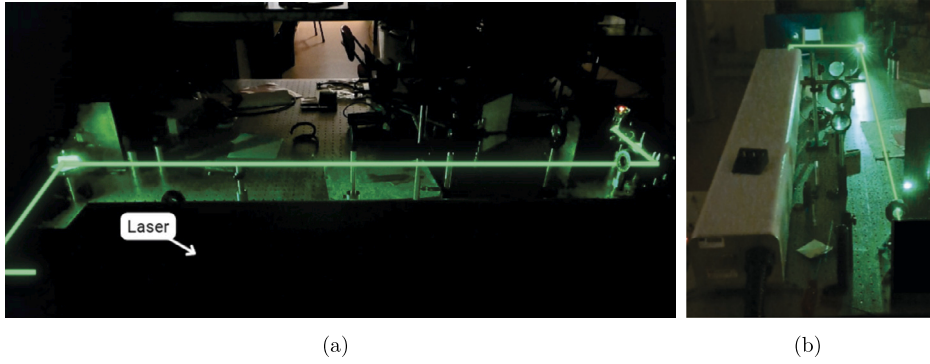
(a)   (b)

Fig. 3. Solid-state laser used as illumination source with its optical path illustrated from different perspectives.

4.1.2. Detection module

After selecting the most suitable piezoelectric transducers for detecting the PA signals in the reported system, the design of the electronics detection circuit was performed.

The detection module of the PA system uses a PZT-5H piezoelectric transducer with a 27 mm diameter and 500 μm thickness. Its experimental resonance frequencies were around 94 kHz in the radial mode and 4 MHz in the TE mode (section 5.1), characterized using the setup presented in section 3.2.

This transducer was chosen because it is widely used in similar systems [11,19–21] and its favorable electrical characterization, showing good impedance matching and also a linear relationship between emitted and received amplitudes in the experimental characterization.

Following the piezoelectric transducer, a charge amplifier comprising a two-stage differential charge amplifier [18] was used. The first stage was based on a modified Howland circuit to convert differential-mode input to a single-ended signal while rejecting common-mode input. The second stage consisted of a standard current integrator with high-pass filtering outputted a single-ended voltage. This setup offers low noise and high sensitivity, enhancing the signal to noise ratio (SNR). Gain adjustment was achieved by regulating resistors R_a and R_b [22] (in this work, a gain of 46 dB was used). Grounded resistors were connected to each amplifier input in the first stage to supply the necessary bias current. This amplifier was implemented using the IC LT1259 (Analog Devices), supplied by a 5V DC power supply. Matching conditions for proper amplifier operation are detailed in Equation (9) and Fig. 4 (a).

$$\begin{cases} R_1 = R \\ R_2 = R_a + R_b = R \end{cases} \tag{9}$$

with

$$\begin{cases} R_a = (1-a)R \\ R_b = aR \\ 0 < a \le 1 \end{cases}$$

For this charge amplifier, its differential gain (G_D) and sensitivity (S_Q) are given according to Equations (10) and (11):

$$G_D = \frac{2}{a} \frac{sR_f}{1 + sR_f C_f} \tag{10}$$

$$S_Q = \frac{2}{a} \frac{1}{C_f} \tag{11}$$

It can be verified that reducing the value of a leads to an increase in both differential gain and sensitivity. This can be achieved by increasing R_a and decreasing R_b while decreasing C_f also boosts sensitivity. The chosen circuit values resulted in a low a value ($a \sim 0.33$). To meet low pole frequency requirements, high C_f and R_f values are recommended, but low noise and high sensitivity require a low C_f. Thus, a high R_f and low C_f were chosen.

Secondly, a passive Twin-T notch filter was implemented to remove power-line interferences, with a 50 Hz cut-off frequency (f_N) as projected in Equation (12) (Fig. 4 (a)).

$$f_N = \frac{1}{4\pi RC} \tag{12}$$

Finally, an active band-pass filter (Fig. 4 (a)) was implemented with a lower cut-off frequency (f_L) of 15.9 kHz and an upper cut-off frequency (f_H) of approximately 5.3 MHz to attenuate very low and very high frequencies. The TL084CN IC (Texas Instruments) was chosen for the band-pass filter, and this IC was supplied with DC voltages of ± 15 V.
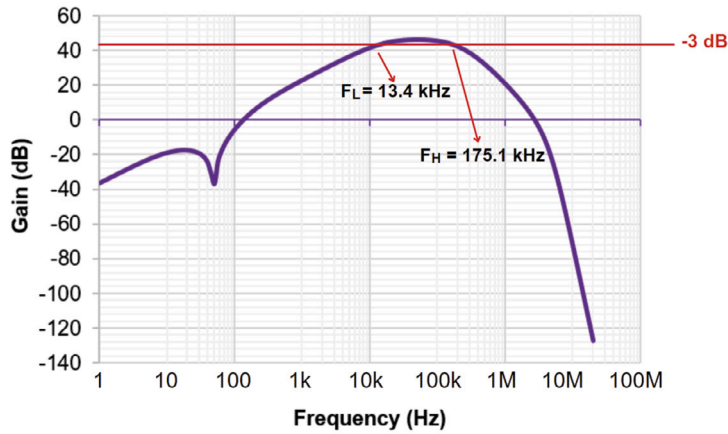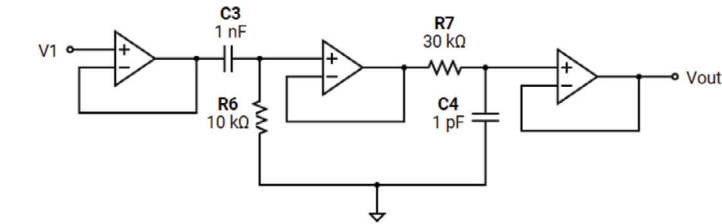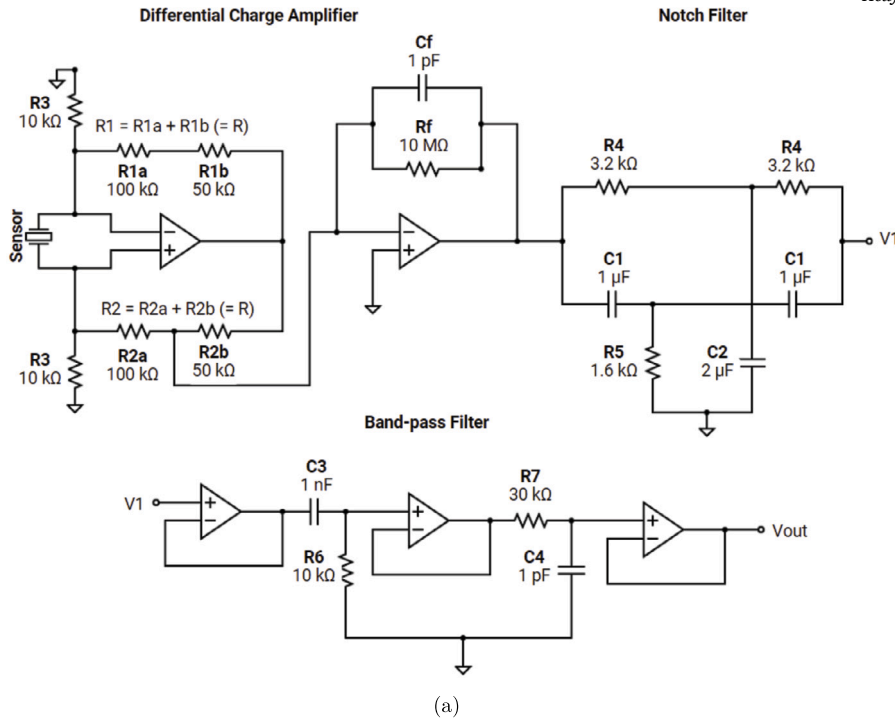
**Fig. 4.** (a) Schematic and (b) Bode plot of the detection circuit.

Both the upper and lower cut-off frequencies were calculated according to the Equation (13):

$$f_c = \frac{1}{2\pi RC} \tag{13}$$

The complete detection circuit is represented in Fig. 4 (a).

Simulation on LTspice software analyzed the circuit's Bode plot, as shown in Fig. 4 (b). Nevertheless, it is essential to recognize that this graph represents an estimation of the circuit's actual performance, since it was not tested with the PZT transducer. However, the obtained curve displays a significant decrease near 50 Hz, which aligns with the response of the notch filter. The increase continues until it hits a peak of 46 dB. It is important to point out that around 13.4 kHz, there is a reduction of -3 dB from the maximum gain, which corresponds closely to the lower cut-off frequency that was set for the band-pass filter. The upper cut-off frequency is around 175.1 kHz, which is lower than the designed cut-off frequency for the band-pass filter, which is attributed mainly to the Gain x Bandwidth product.

Overall, the circuit has a substantial gain of 46 dB and a bandwidth of around 161.7 kHz, meeting the necessary characteristics for detecting PA signals from biomolecules (frequency around 100 kHz for hemoglobin), since even if it is necessary to detect in the
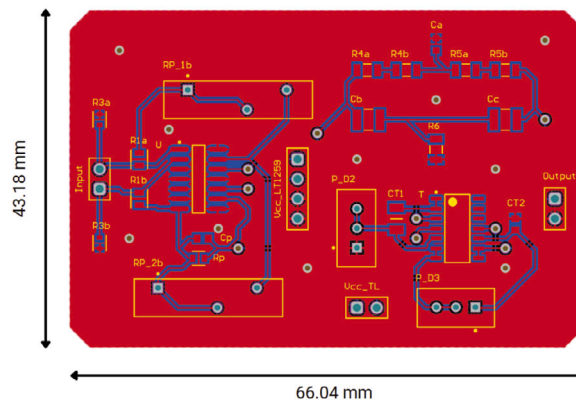
(a)
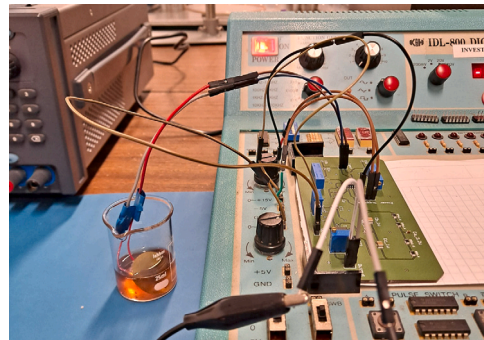
(b)

Fig. 5. (a) Schematic of the PCB (b) PCB connected to the PZT transducer.

Table 1
Theoretical resonance frequencies calculated in different modes.

Mode	Thickness	Resonance Frequency
TE	500 um	3.98 MHz
Radial	27 mm	73.3 kHz

range of a few MHz, the circuit has enough gain. Furthermore, it should be noted that the gain can be easily adjusted by varying R_a and R_b as required, with the circuit achieving a maximum gain of approximately 100 dB.

The developed circuit design was implemented on a fabricated PCB to obtain a more robust and compact circuit. Fig. 5 presents the design (Fig. 5 (a)) and the fabricated PCB connected to the PZT transducer (Fig. 5 (b)) of the developed circuit.

5. Results and discussion

5.1. Piezoelectric transducer characterization

The following subsections present the results obtained from the measurements and characterization of the piezoelectric PZT-5H transducer chosen for the PA system's detection module.

5.1.1. Theoretical characterization

Firstly, it was calculated the theoretical resonance frequency of the PZT-5H disk transducer, both in the thickness and radial directions. For this calculus, it was considered the thickness and radius of the transducer, as well as the sound speed 3.98×10^3 m/s of the PZT-5H material [17,23].

Hence, Equation (8) was solved, obtaining the resonance frequency values presented in Table 1. In the thickness extensional (TE) mode, the thickness value corresponds to the thickness of the transducer, whereas in the radial mode, the thickness value equals the transducer's diameter. The predicted values show that, as expected, the TE resonant frequency is considerably superior to the radial one.
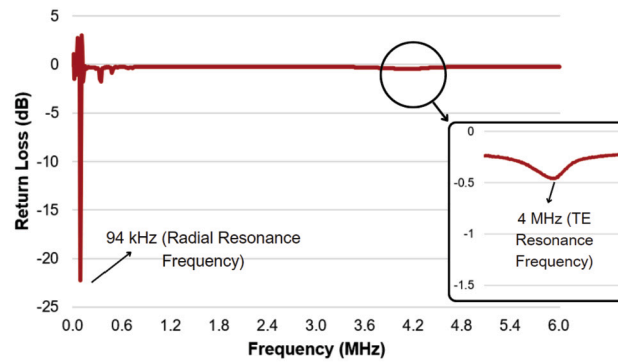
Fig. 6. Return loss variation according to frequency for the PZT-5H transducer from 10 kHz to 6 MHz.

Table 2
The amplitude of the detected wave varies according to the amplitude of the transmitted wave.

Emitting transducer amplitude (V)	Receiving transducer amplitude (mV)	σ (mV)
0.100	19.867	0.377
0.200	34.533	1.050
0.500	79.733	0.377
1.000	154.667	0.943
2.000	301.333	1.886
3.000	452.000	0.000
4.000	593.333	1.886
5.000	752.000	0.000

As the transducers vibrate in a direction perpendicular to their thickness, they expand and contract in that direction during for each oscillation cycle. Oscillating in the TE mode causes greater deformation and requires less energy, ultimately leading to a higher stiffness when compared to the radial mode. Because the radial mode requires greater energy and has lower stiffness, the resonance frequency is lower in this orientation than in the thickness orientation [17].

5.1.2. Electrical characterization

The electrical characterization of the PZT-5H piezoelectric transducer was performed by measuring the S-parameters from 10 kHz to 6 MHz, without using an impedance matching circuit, in order to determine the return loss (RL), which indicates the reflected electrical power. During the measurements, the transducer was immersed in water. Since water and PZT have similar acoustic impedance values ($Z = 1.48 \times 10^6\ Kg/m^2 s$ and $Z = 31 \times 10^6\ Kg/m^2 s$, respectively) compared to air ($Z = 400\ Kg/m^2 s$), this results in improved acoustic matching and reduced reflection of acoustic waves at the transducer-medium interface, allowing for more efficient sound wave propagation [17].

In Fig. 6, the RL spectrum of the PZT-5H transducer is presented, regarding to the frequency.

Therefore, it was demonstrated that the PZT-5H transducer exhibits significantly lower RL peak levels at 94 kHz (approximately -22 dB) and 4 MHz (around -0.5 dB), corresponding to the radial and TE resonance frequencies, respectively. The values closely resemble the theoretical values previously discussed and represent the highest electrical transmission capability of the PZT transducer. Moreover, it can be noted that the transducer exhibits higher efficiency at the radial resonance frequency as opposed to the TE resonance frequency, as the RL value is much lower at 94 kHz. It is also noteworthy that the peaks occurring after the radial resonance frequency represent the harmonics of the signal.

5.1.3. Experimental characterization

Sine waves were used during the experimental characterization to serve as input signals for the emitter transducer. The transducers were evaluated at the radial resonance frequency, which is the frequency at which the RL value is the lowest. Amplitude variations from 10 mV to 5 V were applied to the emitted wave, with the receiver placed 2 cm away. Table 2 and Fig. 7 illustrate the nearly linear connection between the emitted and received wave amplitudes. For instance, when the emitted wave has an amplitude of 1V, the received wave's amplitude is around 160 mV.

Then, the transducers were shifted to determine how the wave's amplitude changes with the distance between them. Sine waves were produced at amplitudes spanning from 100 mV to 5 V, at the radial resonance frequency, and at distances of 1, 2, 4, and 6 cm. In Fig. 8 and Table 3, it can be seen that the intensity of the received wave decreases as the gap between transducers increases (with variable emitting wave amplitudes), with a more pronounced decline at shorter distances that stabilizes as the distance from the transducer increases. Accordingly, the amplitude variations based on distance were deemed not significant due to the relatively low attenuation coefficient [17].
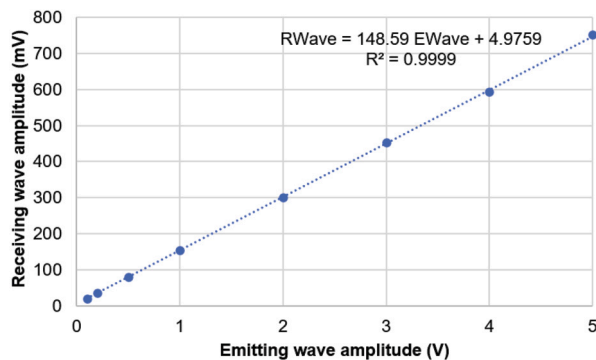
Fig. 7. The amplitude of the received wave varies depending on the amplitude of the emitted wave.

Table 3

Variation of the received wave amplitude as a function of the distance between transducers, for different emitting wave amplitudes.

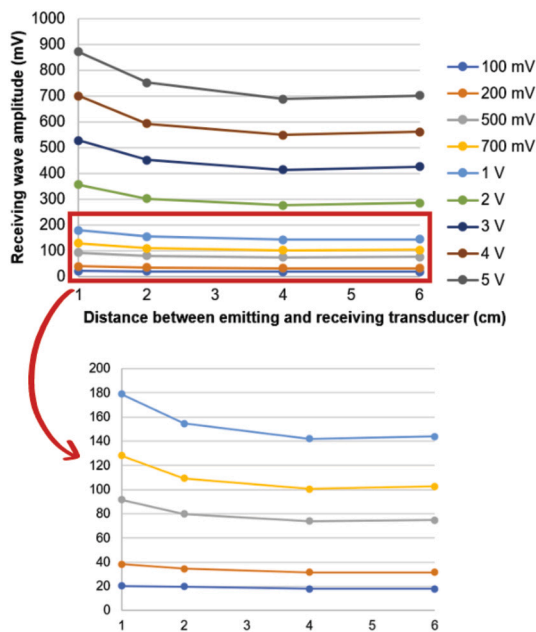| Distance \ E. amplitude	100 mV	σ (mV)	200 mV	σ (mV)	500 mV	σ (mV)	700 mV	σ (mV)
1	20.400	0.400	38.400	0.400	91.600	0.400	128.000	0.000
2	19.867	0.377	34.533	1.050	79.733	0.377	109.333	0.471
4	17.867	0.680	31.600	0.327	73.867	0.377	100.400	1.178
6	18.000	0.653	31.533	0.411	74.867	0.340	102.667	0.943

*E. amplitude: Emitting amplitude.

Fig. 8. The amplitude of the received wave varies depending on the distance separating the PZT disks, for various emitted wave amplitudes.

5.2. Hemoglobin photoacoustic detection

Fig. 9 displays the mean of ten measurements of the PA signals from a sample of distilled water and of three hemoglobin concentrations.

The initial peaks generated for each sample are present due to electrical interference when the laser is activated, as shown in Fig. 9, i.e., even when the laser is focused on a distilled water sample, the initial peak is also present, even though water does not produce a PA response (at this wavelength). Thus, for all samples, this first peak was neglected when evaluating the PA signal.

By examining the curves of Figs. 9 and 10, it was noted that more concentrated hemoglobin solutions yielded stronger responses, consistent with theory. Therefore, a maximum amplitude of approximately 44 mV was obtained for the 10 mg/mL solution. Furthermore, as shown in Fig. 10, it is observed a practically linear relationship between amplitude and hemoglobin concentration.
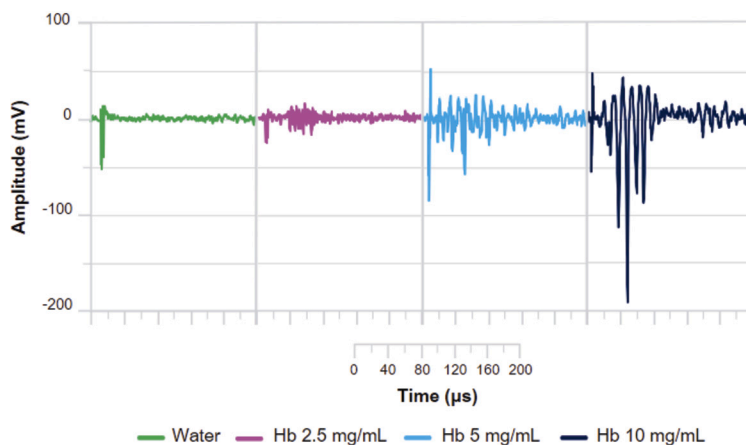
Fig. 9. Curves obtained for a distilled water sample and three hemoglobin solutions of different concentrations (n = 10).
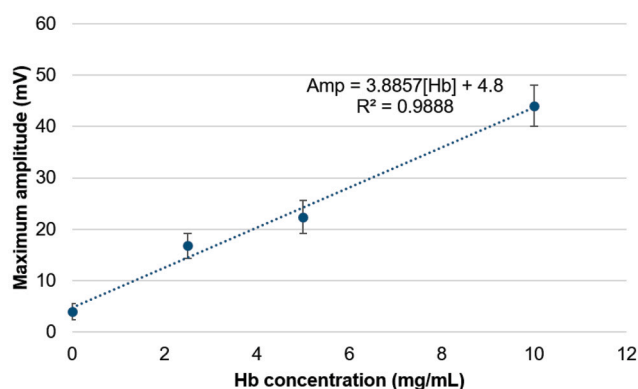

Fig. 10. Maximum amplitude (mV) of the photoacoustic signal, for varying hemoglobin concentrations (mg/mL) in the sample.

The waves that follow the PA signals correspond to acoustic reflections that occur in the wall of the goblet since only a single laser pulse was emitted. These reflections are more noticeable in the 10 mg/mL curve (Fig. 9).

Considering that the majority of PA systems designed for similar purposes focus on identifying hemoglobin in blood samples [3,15,24–26], the unique capability of our system to detect hemoglobin even at extremely low levels is noteworthy. This can be stated since blood has minimum concentrations of hemoglobin of approximately 120 mg/mL [4,27], while our system was able to detect minimum concentrations of 2.5 mg/mL, which is 48 times lower.

The estimated detection limit of the developed sensor was 1.24 mg/mL, as extrapolated from the linear trend of Fig. 10 (based on the noise-signal ratio). Although the actual prototype performance allows measuring these ranges in whole blood, its total measurement range and detection limit can be improved to lower values by adjusting the gain implemented in the charge amplifier circuit. In fact, this possibility can be very useful in applications where low levels of Hb are presented, such as in serum, or other fluids under testing in organ-on-a-chip devices (in these devices, typically lower hematocrit ranges are considered, generally up to 2%) [4,27].

6. Towards the integration of a photoacoustic system in organ-on-a-chip

After the previous validation, it was projected an integration possibility for the designed photoacoustic detection system into an organ-on-a-chip platform. The integrated system comprises the OoC microfluidic device, which is used to host the cellular cultures and perform organoid studies, and is connected to a fluidic channel that pumps the sample up to the detection chamber. When the Hb fluidic samples reach this chamber, the nanosecond laser (external to the OoC platform) is focused and the photoacoustic response will be acquired. In addition, the system includes a transparent optical window, where the excitation light will irradiate the sample; and the piezoelectric transducer, responsible for obtaining the photoacoustic signal. The excitation light and the acoustic transducer will be positioned in a 90° configuration, to prevent the transducer from being directly irradiated by the excitation light. In the integration phase, a transducer with a similar resonance frequency to those studied, but with smaller dimensions, will be used. A good candidate is a piezoelectric disc with an outside diameter of 5 mm and a thickness of 0.25 mm (PRYY+0398 from PImicos), which can be placed and aligned on the fluidic substrate (fully submerged during measurements).
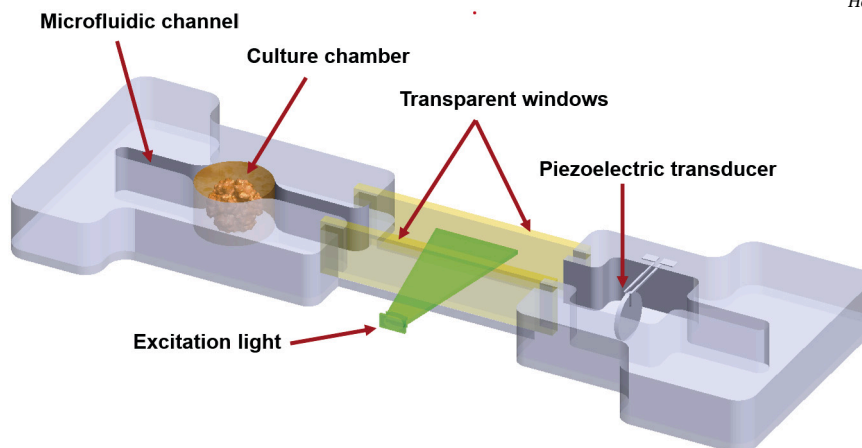
Fig. 11. Schematic illustration of an ideal photoacoustic detection system integrated into an organ-on-a-chip for Hb monitoring.

The microfluidic die of the organ-on-a-chip was already designed and optimized in previous works of our team [28]. This microfluidic die will be fabricated in biocompatible and transparent polydimethylsiloxane (PDMS), using molds of polymethylmethacrylate (PMMA) obtained by laser cutting.

A schematic representation of the targeted integrated portable and compact platform is shown in Fig. 11.

7. Conclusion

This paper presents the development of an electronic detection circuit for a PA system, aiming to integrate it into an OoC.

To this end, a piezoelectric transducer was first characterized theoretically, electrically and experimentally in order to understand its mechanical and electrical behavior. Next, the detection system was developed, based on a differential charge amplifier which, connected to the PZT transducer, acquired and processed the PA signal. The system was finally validated using an Nd:YAG laser as the illumination source, emitting at 532 nm wavelength, to excite the hemoglobin samples and trigger the PA effect. Hemoglobin samples of different concentrations, as low as 2.5 mg/mL, were easily detected.

The results obtained showed that higher PA signal amplitudes were obtained for more concentrated solutions of hemoglobin. In addition, the good performance of the electronic detection circuit developed stands out, as does its ability to detect hemoglobin in very low concentrations, down to 2.5 mg/mL. However, it is also possible to detect higher concentrations reducing the gain to avoid saturation of the detection system developed.

Therefore, as future work, we intend to move towards integrating the developed system into an OoC. Hence, following this proof-of-concept, showing that we can detect low hemoglobin concentrations, we will transition to the use of micromachined ultrasound transducers along with an integrated and miniaturized detection system. Afterward, it is desirable to upgrade the illumination source to a more compact and cheaper option, such as a laser diodes or LEDs, and develop the proper actuation circuit to make the PA system portable, able to be integrated into a OoC platform.

CRediT authorship contribution statement

Bruna Pinheiro: Writing – original draft, Validation, Methodology, Investigation, Conceptualization. **Vânia Pinto:** Writing – review & editing, Methodology, Investigation, Conceptualization. **Hugo Dinis:** Validation, Methodology, Conceptualization. **Michael Belsley:** Writing – review & editing, Resources, Methodology. **Susana Catarino:** Writing – review & editing, Methodology, Conceptualization. **Graça Minas:** Writing – review & editing, Validation, Supervision, Conceptualization. **Paulo Sousa:** Writing – review & editing, Validation, Supervision, Resources, Project administration, Methodology, Investigation, Funding acquisition, Formal analysis, Conceptualization.

Declaration of competing interest

The authors declare that they have no known competing financial interests or personal relationships that could have appeared to influence the work reported in this paper.

Data availability statement

The data supporting this study's findings are available from the corresponding author upon request.

References

[1] C.M. Leung, et al., A guide to the organ-on-a-chip, Nat. Rev. Methods Primers 2 (1) (Dec. 01, 2022), https://doi.org/10.1038/s43586-022-00118-6, Springer Nature.

[2] Q. Wu, et al., Organ-on-a-chip: recent breakthroughs and future prospects, Biomed. Eng. Online 19 (1) (Feb. 2020) 1–19, https://doi.org/10.1186/S12938-020-0752-0.

[3] E. Koushki, R. Tayebee, M. Esmaeili, Nonlinear optical and photoacoustic properties of aqueous crystalline hemoglobin. Towards facile detection of hemoglobin concentration in blood, J. Mol. Liq. 325 (Mar. 2021), https://doi.org/10.1016/j.molliq.2020.115169, ISSN: 01677322.

[4] R. Ranjith, S. Priya, A.S. Kaviya, J.B. Jeeva, Non-invasive hemoglobin measurement using optical method, Heliyon 10 (15) (Aug. 2024) e35777, https://doi.org/10.1016/j.heliyon.2024.e35777.

[5] A. Barati, M. Shamsipur, H. Abdollahi, Hemoglobin detection using carbon dots as a fluorescence probe, Biosens. Bioelectron. 71 (Sep. 2015) 470–475, https://doi.org/10.1016/j.bios.2015.04.073, ISSN: 18734235.

[6] X. Yang, Y.-H. Chen, F. Xia, M. Sawan, Photoacoustic imaging for monitoring of stroke diseases: a review, Photoacoustics 23 (Sep. 2021) 100287, https://doi.org/10.1016/j.pacs.2021.100287.

[7] R.D. Whitehead, Z. Mei, C. Mapango, M.E.D. Jefferds, Methods and analyzers for hemoglobin measurement in clinical laboratories and field settings, Ann. N.Y. Acad. Sci. 1450 (1) (Aug. 2019) 147–171, https://doi.org/10.1111/nyas.14124.

[8] M. Li, Y. Tang, J. Yao, Photoacoustic tomography of blood oxygenation: a mini review, Photoacoustics 10 (Jun. 2018) 65–73, https://doi.org/10.1016/j.pacs.2018.05.001.

[9] L.v. Wang, L. Gao, Photoacoustic microscopy and computed tomography: from bench to bedside, Annu. Rev. Biomed. Eng. 16 (2014) 155–185, https://doi.org/10.1146/annurev-bioeng-071813-104553, Annual Reviews Inc.

[10] L.V. Wang, J. Yao, A practical guide to photoacoustic tomography in the life sciences, Nat. Methods 13 (8) (Jul. 28, 2016) 627–638, https://doi.org/10.1038/nmeth.3925, Nature Publishing Group.

[11] C. Yang, X. Jian, J. Lv, Z. Han, G. Sergiadis, Y. Cui, Highly Sensitive PZT Transducer with Integrated Miniature Amplifier for Photoacoustic Imaging, ISBN 9781728145969, Oct. 2019, p. 2644.

[12] M.K.A. Singh, W. Xia, Portable and affordable light source-based photoacoustic tomography, Sensors (Switzerland) 20 (21) (Nov. 01, 2020) 1–29, https://doi.org/10.3390/s20216173, MDPI AG.

[13] E.M. Strohm, M.J. Moore, M.C. Kolios, Single cell photoacoustic microscopy: a review, IEEE J. Sel. Top. Quantum Electron. 22 (3) (May 01, 2016) 137–151, https://doi.org/10.1109/JSTQE.2015.2497323, Institute of Electrical and Electronics Engineers Inc.

[14] R. Gao, Z. Xu, Y. Ren, L. Song, C. Liu, Nonlinear mechanisms in photoacoustics—powerful tools in photoacoustic imaging, Photoacoustics 22 (Jun. 2021) 100243, https://doi.org/10.1016/j.pacs.2021.100243.

[15] X. Wang, X. Xie, G. Ku, L.V. Wang, G. Stoica, Noninvasive imaging of hemoglobin concentration and oxygenation in the rat brain using high-resolution photoacoustic tomography, J. Biomed. Opt. 11 (2) (2006) 024015, https://doi.org/10.1117/1.2192804.

[16] D. Halliday, R. Resnick, J. Walker, Fundamentals of Physics, 10th ed., Wiley, 2013.

[17] B.R. Pinheiro, H.D. Dinis, S.O. Catarino, V.C. Pinto, P.J. Sousa, G. Minas, Experimental characterization of a piezoelectric transducer for integration into a photoacoustic system, in: 2023 IEEE 7th Portuguese Meeting on Bioengineering (ENBENG), IEEE, Jun. 2023, pp. 84–87.

[18] A. Kamnaksh, N. Puhakka, I. Ali, G. Smith, R. Aniceto, J. McCullough, S. Das Gupta, X.E. Ndode-Ekane, R. Brady, P. Casillas-Espinosa, M. Hudson, C. Santana-Gomez, R. Immonen, P.A. Abreu, N. Jones, S. Shultz, R.J. Staba, T.J. O'Brien, D. Agoston, A. Pitkänen, Harmonization of pipeline for preclinical multicenter plasma protein and miRNA biomarker discovery in a rat model of post-traumatic epileptogenesis, Epilepsy Res. 149 (2019 Jan) 92–101, https://doi.org/10.1016/j.eplepsyres.2018.11.009. Epub 2018 Nov 26. PMID: 30553097; PMCID: PMC6326854.

[19] K. Roy, et al., Body conformal linear ultrasound array for combined ultrasound and photoacoustic imaging, in: IEEE International Ultrasonics Symposium, IUS, IEEE Computer Society, Sep. 2020.

[20] A. Dangi, S. Agrawal, J. Lieberknecht, J. Zhang, S.R. Kothapalli, Ring ultrasound transducer based miniaturized photoacoustic imaging system, in: Proceedings of IEEE Sensors, Institute of Electrical and Electronics Engineers Inc., Dec. 2018.

[21] R. Sasaki, S. Kino, Y. Matsuura, Mid-infrared photoacoustic spectroscopy based on ultrasound detection for blood component analysis, Biomed. Opt. Express 14 (7) (Jul. 2023) 3841, https://doi.org/10.1364/boe.494615.

[22] M. Massarotto, A. Carlosena, A.J. Lopez-Martin, Two-stage differential charge and transresistance amplifiers, IEEE Trans. Instrum. Meas. 57 (2) (Feb. 2008) 309–320, https://doi.org/10.1109/TIM.2007.909498.

[23] S.O. Catarino, L.R. Silva, P.M. Mendes, J.M. Miranda, S. Lanceros-Mendez, G. Minas, Piezoelectric actuators for acoustic mixing in microfluidic devices - numerical prediction and experimental validation of heat and mass transport, Sens. Actuators B, Chem. 205 (Dec. 2014) 206–214, https://doi.org/10.1016/j.snb.2014.08.030.

[24] A. Danielli, C.P. Favazza, K. Maslov, L.V. Wang, Picosecond absorption relaxation measured with nanosecond laser photoacoustics, Appl. Phys. Lett. 97 (16) (Oct. 2010), https://doi.org/10.1063/1.3500820.

[25] L. De Liao, et al., Imaging brain hemodynamic changes during rat forepaw electrical stimulation using functional photoacoustic microscopy, NeuroImage 52 (2) (Aug. 2010) 562–570, https://doi.org/10.1016/J.NEUROIMAGE.2010.03.065.

[26] Y. Zhu, et al., Light emitting diodes based photoacoustic imaging and potential clinical applications, Sci. Rep. 8 (1) (Jun. 2018) 1–12, https://doi.org/10.1038/s41598-018-28131-4.

[27] A. Wahed, A. Dasgupta, Red blood cell disorders, in: Hematology and Coagulation, Elsevier, 2015, pp. 31–53.

[28] V. Carvalho, et al., Numerical evaluation and experimental validation of fluid flow behavior within an organ-on-a-chip model, Comput. Methods Programs Biomed. 243 (Jan. 2024) 107883, https://doi.org/10.1016/j.cmpb.2023.107883.